THE JOURNAL OF BIOLOGICAL CHEMISTRY VOL. 286, NO. 39, pp. 34382–34390, September 30, 2011

Functional Role of Two Interhelical Disulfide Bonds in Human Cox17 Protein from a Structural Perspective*[S]

Received for publication, March 31, 2011, and in revised form, August 2, 2011 Published, JBC Papers in Press, August 4, 2011, DOI 10.1074/jbc.M111.246223

Lucia Banci, Ivano Bertini[1], Chiara Cefaro, Simone Ciofi-Baffoni, and Angelo Gallo

From the Magnetic Resonance Center Centro Risonanze Magnetiche and Department of Chemistry, University of Florence, Via Luigi Sacconi 6, 50019 Sesto Fiorentino, Florence, Italy

Background: Human Cox17 consists of a α-hairpin domain stabilized by two disulfide bonds.
Results: The disulfide bond, formed by Cys-36 and Cys-45, stabilizes interhelical hydrophobic interactions, whereas the other formed by Cys-26 and Cys-55 is important for structurally organizing the nearby copper-binding site region.
Conclusion: The two disulfide bonds have different functional roles.
Significance: These data contribute to elucidate the oxidative folding mechanism of Cox17.

Human Cox17 is the mitochondrial copper chaperone responsible for supplying copper ions, through the assistance of Sco1, Sco2, and Cox11, to cytochrome *c* oxidase, the terminal enzyme of the mitochondrial energy-transducing respiratory chain. It consists of a coiled coil-helix-coiled coil-helix domain stabilized by two disulfide bonds and binds one copper(I) ion through a Cys–Cys motif. Here, the structures and the backbone mobilities of two Cox17 mutated forms with only one interhelical disulfide bond have been analyzed. It appears that the inner disulfide bond (formed by Cys-36 and Cys-45) stabilizes interhelical hydrophobic interactions, providing a structure with essentially the same structural dynamic properties of the mature Cox17 state. On the contrary, the external disulfide bond (formed by Cys-26 and Cys-55) generates a conformationally flexible α-helical protein, indicating that it is not able to stabilize interhelical packing contacts, but is important for structurally organizing the copper-binding site region.

Disulfide bond formation *in vivo* requires dedicated proteins that act as catalysts to allow rapid folding of the nascent protein (1, 2). Several cysteine-rich proteins containing a twin CX_9C motif are targeted to the intermembrane space (IMS)[2] of the mitochondria and, once imported in the IMS, undergo an oxidative folding process guided by a protein machinery that introduces disulfide bond(s) in these proteins (3–5). Mia40 is an essential protein of this machinery and works as an oxidoreductase and molecular chaperone to cause both disulfide bond formation (6–8) and folding of the substrate (9). One of the best characterized substrates of Mia40 is the mitochondrial protein Cox17, which contains a twin CX_9C motif and a Cys-Cys motif at the N terminus involved in copper(I) binding (10–14). Once imported into the IMS, Mia40 recognizes an IMS-targeting signal of Cox17 via hydrophobic interactions that determine the formation of a specific, transient intermolecular disulfide intermediate with Mia40 (15). These interactions induce the formation of an α-helix in the IMS-targeting signal-containing segment of Cox17 located between the two cysteines of the second (in sequence) CX_9C motif (9). An intramolecular disulfide bond within Cox17 (connecting the inner cysteines of the $CX_9\underline{\mathbf{C}}$-$\underline{\mathbf{C}}X_9C$ motif) is then formed with Cox17 released from Mia40 (6, 9). Once the intramolecular disulfide bond is formed, Cox17 undergoes the formation of a second α-helical segment involving the residues between the two cysteines of the first (in sequence) CX_9C motif (9). Finally, the formation of the second disulfide bond connecting the outer cysteines of the $\underline{\mathbf{C}}X_9C$-$CX_9\underline{\mathbf{C}}$ motif occurs. Under aerobic, *in vitro* conditions, oxygen can rapidly form the second disulfide bond in an already folded protein (6), or, under anaerobic *in vitro* conditions and in the presence of an excess of Mia40, another molecule of Mia40 can rapidly oxidize the second disulfide bond (16). These or others possibilities could occur *in vivo* for completing Cox17 maturation. The Mia40-catalyzed oxidative folding process of Cox17 determines the formation of a coiled coil-helix-coiled coil-helix (CHCH) domain stabilized by two disulfide bonds and preceded by a flexible and completely unstructured N-terminal tail containing the CC motif in its reduced state ($Cox17_{2S\text{-}S}$ hereafter) (10, 12). These findings are consistent with the reduction potentials available in the literature (6, 17). The latter $Cox17_{2S\text{-}S}$ state binds a copper(I) ion with high affinity (18), and it has been proposed to act as a mitochondrial copper chaperone in the IMS, supplying copper(I) ions through the assistance of Sco1, Sco2, and Cox11 to cytochrome *c* oxidase (19, 20). According to this proposal, it has been indeed found that *in vitro* $Cu(I)Cox17_{2S\text{-}S}$ transfers the Cu(I) ion to

* This work was supported by WeNMR Project (European FP7 e-Infrastructure grant, Contract 261572), supported by the national GRID initiatives of Belgium, Italy, Germany, The Netherlands (via the Dutch BiG Grid project), Portugal, the United Kingdom, South Africa, and the Latin America GRID infrastructure via the Gisela and by the Italian FIRB PROTEOMICA MIUR Contract RBRN07BMCT. Molecular graphics images were produced using the UCSF Chimera (39) package from the Resource for Biocomputing, Visualization, and Informatics at the University of California, San Francisco, supported by United States National Institutes of Health Grant P41 RR-01081.
[S] The on-line version of this article (available at http://www.jbc.org) contains supplemental Table S1 and Fig. S1.
The atomic coordinates and structure factors (code 2L6Q) have been deposited in the Protein Data Bank, Research Collaboratory for Structural Bioinformatics, Rutgers University, New Brunswick, NJ (http://www.rcsb.org/).
The resonance assignments were deposited in the Biological Magnetic Resonance Bank under accession number 17821.
[1] To whom correspondence should be addressed. Tel.: 39-055-4574272; Fax: 39-055-4574271; E-mail: ivanobertini@cerm.unifi.it.
[2] The abbreviations used are: IMS, intermembrane space; CHCH, coiled coil-helix-coiled coil-helix; HSQC, heteronuclear single-quantum coherence.

Sco1, Sco2, and Cox11 (21–23) and that respiratory growth and cytochrome *c* oxidase activity deficiencies in a yeast Cox17-null strain are reversed by the addition of 0.4% copper salts to the growth medium (24).

To investigate the functional role of the two structural disulfides present in the CHCH domain of Cox17, we have structurally and dynamically characterized two double cysteine mutants of human Cox17, C36S/C45S Cox17 ($hCox17_{outer}$) and C26S/C55S Cox17 ($hCox17_{inner}$) that contain the outer or inner disulfide bond within the twin CX_9C motif, respectively. The structural and backbone dynamic properties of the two mutants are compared with those of wild-type apo-$hCox17_{2S\text{-}S}$. From these data, we conclude that the inner disulfide bond is the essential one to reproduce the same structural-dynamic properties found in the $hCox17_{2S\text{-}S}$ state, whereas the outer disulfide bond controls metal binding site structural environment. These structural data contribute to the elucidation of the Mia40-induced oxidative folding mechanism of Cox17.

EXPERIMENTAL PROCEDURES

Protein Production—Cysteine to serine mutants of hCox17 were generated by PCR-based site-directed mutagenesis (QuikChange site-directed mutagenesis kit; Stratagene) from pETG-30A plasmid containing the hCox17 gene. hCox17 mutants were expressed in *Escherichia coli* BL21-Origami(DE3) cells (Stratagene) and purified following a previously described protocol (10). hCox17 proteins expressed following this procedure contain four additional amino acids (GSFT) corresponding to the tobacco etch virus protease recognition site at the N terminus. In the final step of the purification, the fractions showing a single component by SDS-PAGE were collected, and the protein concentration was measured using the Bradford protein assay. The pure proteins were obtained in their apo state, as checked by inductively coupled plasma MS, and fully oxidized as shown by SDS-PAGE analysis of 4-acetamido-4′-maleimidylstilbene-2,2′-disulfonic acid (AMS)-reacted samples. AMS is a specific cysteine-alkylating agent typically used to follow cysteine redox chemistry modifications (7, 16). In both mutants, reduction of the disulfide bond formed by the two consecutive cysteines, Cys-23 and Cys-24, is almost instantaneous upon addition of equimolar concentration of DTT under nitrogen atmosphere, whereas the structural disulfide bonds remain unaffected by this concentration of reductant, as occurs for the wild-type protein (10). Their reduction potentials are indeed much lower than that of the Cys-23/Cys-24 pair (17). To avoid the formation of a disulfide-bridged dimer caused by Cys-23 and Cys-24 oxidation during the NMR data collection, hCox17 mutants were exchanged under anaerobic conditions into 50 mM phosphate buffer at pH 7.2 using a PD-10 desalting column (Amersham Biosciences) and concentrated by ultrafiltration; DTT was added in a 1:0.7–1.0 protein/DTT ratio to produce the final NMR samples.

NMR Spectroscopy—All of the NMR experiments used for resonance assignment and structure calculations were performed on 0.5–1 mM ^{13}C,^{15}N-labeled samples in 50 mM phosphate buffer, pH 7.2, containing 10% D_2O and DTT. All of the NMR spectra were collected at 298 K, processed using the standard Bruker software (TopSpin 1.3), and analyzed with the CARA program (25). Heteronuclear relaxation experiments were performed on ^{15}N-labeled samples at 500 MHz. The ^{15}N backbone longitudinal (R_1) and transverse (R_2) relaxation rates as well as heteronuclear $^{15}N\{^1H\}$ NOEs were measured as described previously (10).

Structure Calculations—Structure calculations were performed with the software package UNIO, using as input the amino acid sequence, the chemical shift lists, and three ^1H-^1H NOE experiments: two-dimensional NOESY, three-dimensional ^{13}C-edited NOESY, and three-dimensional ^{15}N-edited NOESY recorded at 900 MHz with a mixing time of 100 ms. The standard protocol with seven cycles of peak picking using ATNOS, NOE assignment with CANDID, and structure calculation with CYANA-2.1 was applied (26, 27). φ and ψ dihedral angles were obtained from the chemical shift analysis using the TALOS+ software (28). In each ATNOS/CANDID cycle, the angle constraints were combined with the updated NOE upper distance constraints in the input for the subsequent CYANA-2.1 structure calculation cycle. In the seventh ATNOS/CANDID/CYANA cycle, a total of 1402 or 537 NOE cross-peaks were assigned from 1815 or 789 peaks picked in the spectra of $hCox17_{inner}$ and $hCox17_{outer}$, respectively, which yielded 537 or 183 meaningful NOE upper distance limits. In addition, one disulfide bond between Cys-36 and Cys-45 in the case of $hCox17_{inner}$ and between Cys-26 and Cys-55 in the case of $hCox17_{outer}$ was imposed in the structure calculations. Indeed, the cysteine residues of the twin CX_9C motif, *i.e.* Cys-36, Cys-45 and Cys-26, Cys-55, have $C\beta$ chemical shift values typical of cysteines engaged in disulfide bonds ($C\beta^{36} = 36.6$, $C\beta^{45} = 39.5$ and $C\beta^{26} = 40.6$, $C\beta^{55} = 38.8$) (29). The two cysteines of the Cys-Cys motif are instead reduced in both $hCox17_{inner}$ and $hCox17_{outer}$ mutants ($C\beta$ of Cys-24 = 25.7 and 27.4, respectively).

The 20 conformers of $hCox17_{inner}$ with the lowest target function values were subjected to restrained energy minimization in explicit water with AMBER 10.0 (30). NOE and torsion angle constraints were applied with force constants of 20 kcal mol^{-1} Å^{-2} and 20 kcal mol^{-1} rad^{-2}, respectively. The quality of the structures was evaluated using the Protein Structure Validation Software suite (PSVS) (31) and WHATIF program (32). The conformational and energetic analysis of $hCox17_{inner}$ is reported in supplemental Table S1.

The atomic coordinates, structural restraints, and resonance assignments of $hCox17_{inner}$ have been deposited in the Protein Data Bank (PDB ID code 2LGQ) and BioMagResBank (BRMB ID code 17821).

Copper(I) Binding Characterization—Cu(I)-loaded proteins were first prepared by mixing apo-proteins with 1.5 equivalents of tetrakis(acetonitrile)copper(I) hexafluorophosphate in the presence of equimolar amounts of DTT. DTT and copper(I) excess were then removed in an anaerobic chamber with a PD-10 desalting column. Cu(I)-loaded proteins (20–30 μM) were titrated with the copper(I)-specific competitor BCA in 50 mM phosphate buffer, pH 7.2. The additions were carried out under strictly anaerobic conditions, and the reaction mixture was incubated for 2 h after each addition to attain equilibrium. The reaction progress was monitored by UV/visible spectroscopy by following the increase in the absorption band of

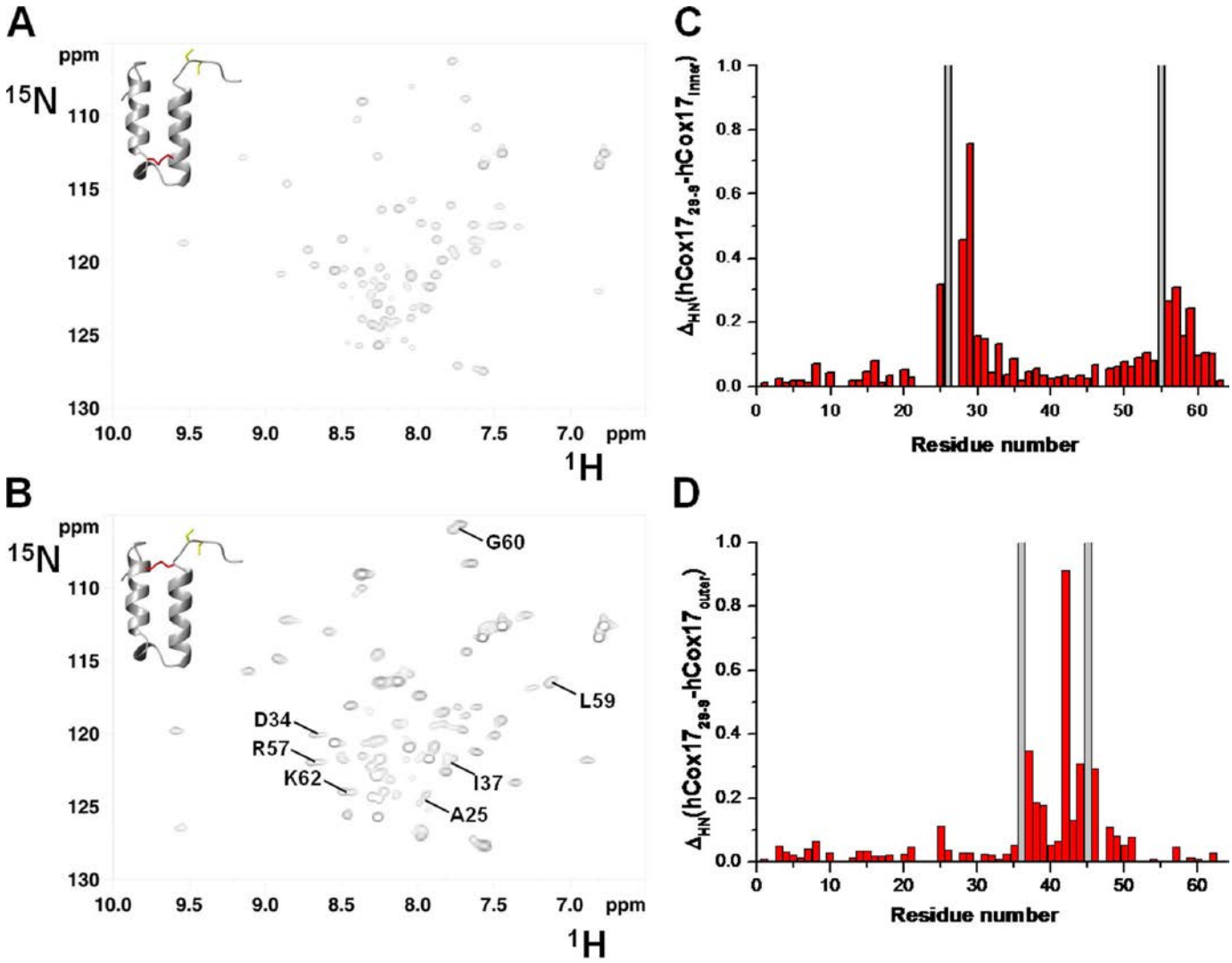

FIGURE 1. *A* and *B*, ^{1}H-^{15}N HSQC maps of apo-hCox17$_{inner}$ (*A*) and apo-hCox17$_{outer}$ (*B*) at 298 K and pH 7.2 in 50 mM phosphate buffer. Some NH cross-peaks of the residues displaying two conformational states in apo-hCox17$_{outer}$ are indicated. In the *insets*, the wild-type apo-hCox17$_{2S\text{-}S}$ structure is displayed in which the outer or inner disulfide bonds are colored in *red* and the cysteines involved in copper(I) binding are in *yellow*. *C* and *D*, weighted average chemical shift differences (Δ_{HN}) between apo-hCox17$_{2S\text{-}S}$ and apo-hCox17$_{inner}$ (*C*), and between apo-hCox17$_{2S\text{-}S}$ and apo-hCox17$_{outer}$ (*D*). $\Delta_{HN} = (((\Delta H)^2 + (\Delta N/5)^2)/2)^{1/2}$, where ΔH and ΔN are chemical shift differences for ^{1}H and ^{15}N, respectively. *Gray bars* identify the positions of Cys → Ser substitutions.

$Cu^{I}(BCA)_2$ at 562 nm. The data were fitted using the program Origin 8.1 following an approach previously reported (33, 34). β_2 for the formation of the Cu(I)$(BCA)_2$ complex was taken as 2.0×10^{17} M^{-1} (35). DTT was also tested as a competitor for both copper(I)-bound mutants to investigate their metal affinity further. However, the amount of DTT needed to extract the copper(I) ion from the mutants prevents metal affinity estimation because of disulfide bond reduction prior to or at the same time as copper(I) removal from hCox17$_{outer}$ and hCox17$_{inner}$, respectively.

^{1}H-^{15}N HSQC experiments were performed on the Cu(I)-bound form of hCox17$_{inner}$ and hCox17$_{outer}$, and backbone chemical shift assignment was performed. Analysis of the chemical shift variations with respect to the corresponding apo-proteins was carried out.

RESULTS

The ^{1}H-^{15}N HSQC spectra of both the hCox17$_{inner}$ and hCox17$_{outer}$ proteins show good NH signal spreading but also a number of signals clustered in the central region (between 8 and 8.5 ppm) of the spectra (Fig. 1, *A* and *B*). This pattern is the same as that observed in the ^{1}H-^{15}N HSQC of wild-type hCox17$_{2S\text{-}S}$ (10) and indicates that hCox17$_{inner}$ and hCox17$_{outer}$ proteins, similar to the wild-type protein, contain both structured and unstructured regions. A backbone resonance assignment of hCox17$_{inner}$ and hCox17$_{outer}$ was accomplished by the analysis of triple resonance experiments. 52 of the expected 55 ^{15}N backbone amide resonances for both hCox17$_{inner}$ and hCox17$_{outer}$ were assigned. The amide resonances are missing for residues Cys-23, Cys-24, and His-47, as occurs for the wild-type apo-protein. The backbone chemical shift values of hCox17$_{inner}$ and hCox17$_{outer}$ compare well with those found for the wild-type protein, with the exception of the residues close to the mutated cysteines (Fig. 1, *C* and *D*). However, at variance with hCox17$_{inner}$ and wild-type hCox17$_{2S\text{-}S}$, in hCox17$_{outer}$ some NHs, located in the vicinity of the Cys-26–Cys-55 disulfide bond, display two conformations as detected in the ^{1}H-^{15}N HSQC map (Fig. 1*C*), indicating the presence of

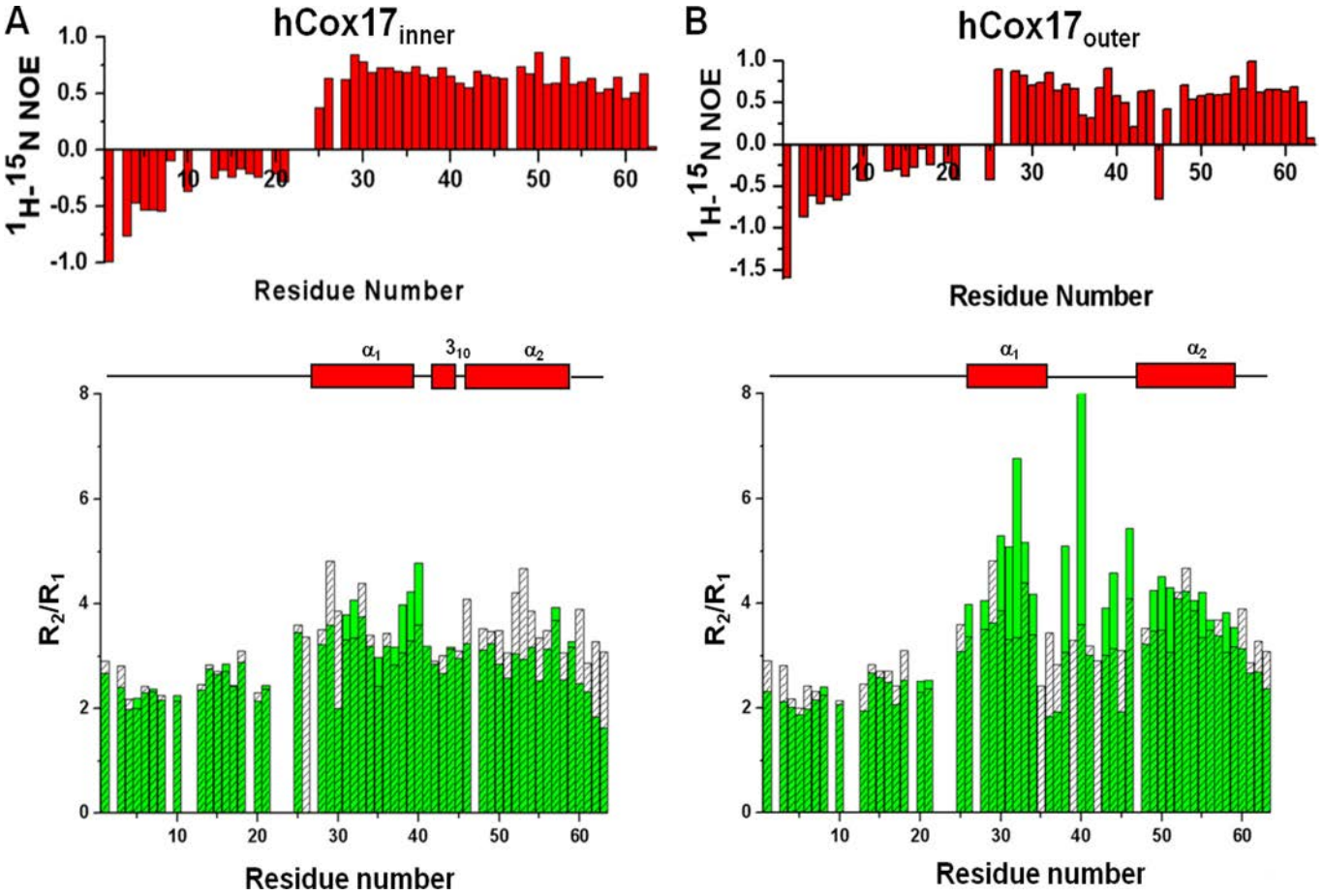

FIGURE 2. **$^{15}N\{^1H\}$ NOEs and ^{15}N R_2/R_1 ratios *versus* residue number of apo-hCox17$_{inner}$ (*A*) and apo-hCox17$_{inner}$ (*B*) collected at 500 MHz in 50 mM phosphate buffer, pH 7.2.** In the two ^{15}N R_2/R_1 plots, *green bars* refer to R_2/R_1 ratios of the inner and outer apo-hCox17 mutants and *white bars* with *hash lines* refers to R_2/R_1 ratios of apo-hCox17$_{2S\text{-}S}$. Reliable relaxation values cannot be obtained for residues 27–28 and 51 because their NH cross-peaks are too broad to be detected in the NMR spectra. Secondary structure elements of apo-hCox17 mutants are indicated at the top of ^{15}N R_2/R_1 plots.

structural heterogeneity in the area surrounding this region. Double conformations could be the result of disulfide bond isomerization, as has already been reported for other systems (36).

The dynamic properties of both hCox17$_{inner}$ and hCox17$_{outer}$ were investigated by measuring longitudinal and transversal relaxation rates and $^{15}N\{^1H\}$ NOEs of the backbone NHs to examine the conformational flexibility of the two proteins, and these data were compared with those of the wild-type apo-hCox17$_{2S\text{-}S}$ protein. The ^{15}N relaxation data show that in both hCox17$_{inner}$ and hCox17$_{outer}$ there are two protein regions with distinctive backbone dynamic regimes, as occurs in the wild-type protein (10): (i) an N-terminal 20-residue stretch characterized by negative $^{15}N\{^1H\}$ NOE values (Fig. 2), indicative of the occurrence of picosecond-nanosecond motions typically present in highly flexible proteins; (ii) the subsequent 25–62 segment which is more rigid with positive $^{15}N\{^1H\}$ NOE values (0.66 ± 0.10; Fig. 2), although the residues in this segment have different degrees of motion when comparing hCox17$_{inner}$ and hCox17$_{outer}$ with hCox17$_{2S\text{-}S}$. Indeed, several residues in the first helix of hCox17$_{outer}$ display R_2/R_1 ratios that are higher than those found for both hCox17$_{2S\text{-}S}$ and hCox17$_{inner}$ (Fig. 2*B*), indicating the presence of chemical exchange phenomena in helix α1 of hCox17$_{outer}$. On the contrary, the hCox17$_{2S\text{-}S}$ and hCox17$_{inner}$ proteins share similar R_2/R_1 ratios in this region (Fig. 2*A*). In addition, the residues following helix α1 in hCox17$_{outer}$ up to the beginning of helix α2 have scattered values for both the R_2/R_1 ratios and the $^{15}N\{^1H\}$ NOE values in comparison with hCox17$_{2S\text{-}S}$ (Fig. 2*B*), indicating the occurrence of backbone motions on both fast nanosecond-picosecond and slow microsecond-millisecond time scales. Overall, the dynamic data analysis supports a model in which the lack of the inner disulfide provokes backbone conformational motions on the first helix and the following loop of the CHCH domain, whereas once this disulfide is present in hCox17$_{inner}$, the dynamic properties of the CHCH domain basically reproduce what occurs when both disulfides are present in hCox17$_{2S\text{-}S}$.

^{13}C resonances of three of the four cysteines have been assigned for both hCox17$_{inner}$ and hCox17$_{outer}$, with ^{13}C chemical shifts missing for Cys-23. The ^{13}C chemical shifts of the $C_{\alpha,\beta}$ atoms of cysteines, which are a clear marker of their oxidation state (29), indicate that Cys-36 and Cys-45 in hCox17$_{inner}$ and Cys-26 and Cys-55 in hCox17$_{outer}$ form a disulfide bond, whereas Cys-24 is in the reduced state in both mutants. Because disulfide-mediated dimerization is prevented for both mutants by the presence of approximately equimolar amounts of protein and DTT (as checked through nonreducing SDS-PAGE), Cys-23 is necessarily in a reduced state. The redox

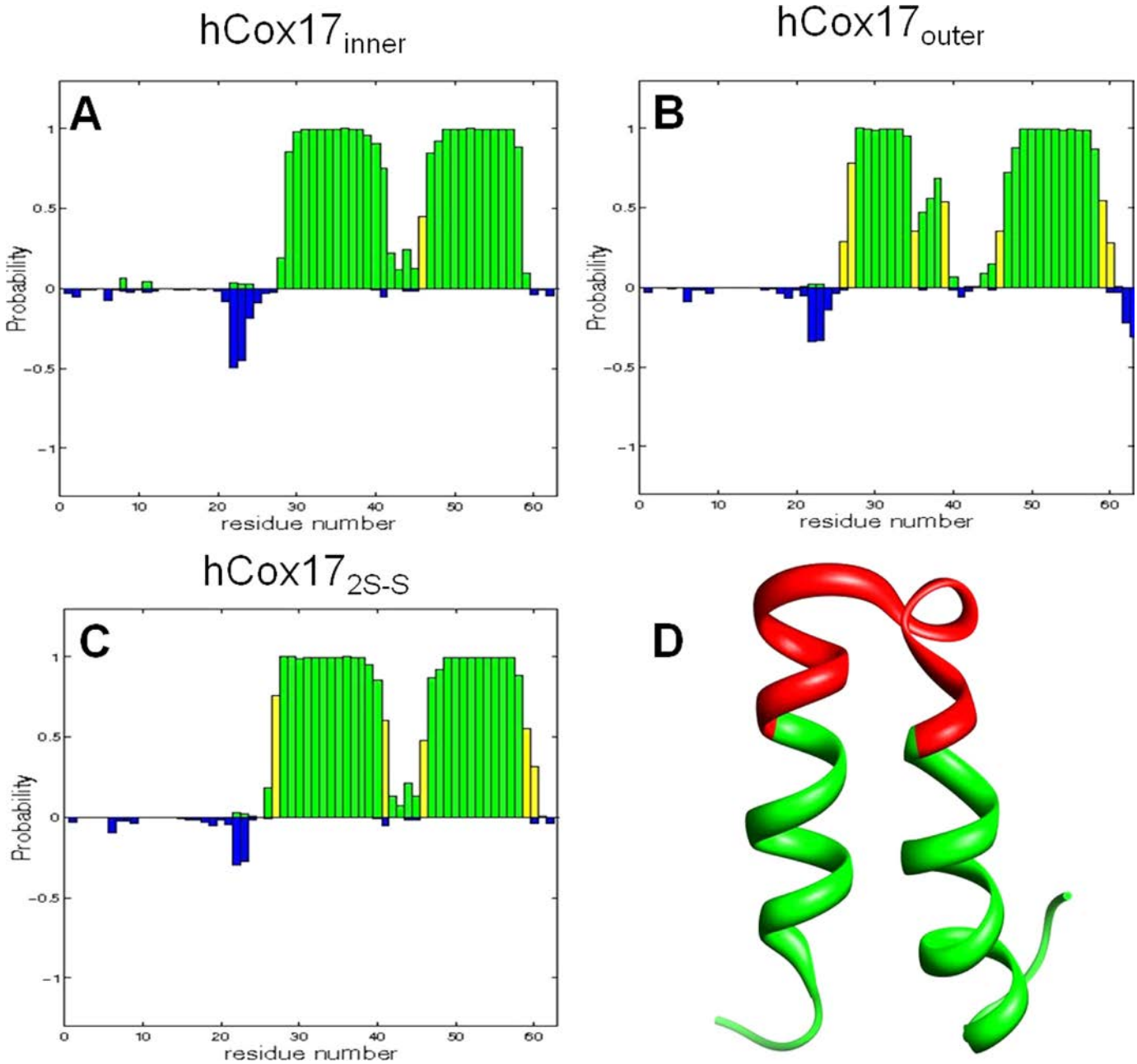

FIGURE 3. *A–C*, secondary structure probability of apo-hCox17$_{inner}$ (*A*), apo-hCox17$_{outer}$ (*B*), and apo-hCox17$_{2S-S}$ (*C*) is derived from chemical shifts using the PECAN program. The *vertical axis* represents the probability of helix (positive, *green*) and of extended structure (negative, *blue*). Values near zero represent random coil residues. The *yellow bars* indicate identification of a region without a distinct structural designation. *D*, residues of hCox17$_{outer}$ showing significant variations in the secondary structural probability with respect to the wild-type protein are mapped in *red* on the solution structure of apo-hCox17$_{2S-S}$.

state of the not-mutated cysteines is therefore unchanged with respect to that of wild-type hCox17$_{2S-S}$ (10).

The structural characterization of both hCox17$_{inner}$ and hCox17$_{outer}$ was performed by solution NMR to investigate how the two disulfide bonds affect the folding properties of hCox17. From the chemical shift index (CSI) (37) and PECAN (38) analysis, it appears that both the hCox17$_{inner}$ and hCox17$_{outer}$ proteins have two helices and an N-terminal unfolded region. The secondary structure prediction profile of hCox17$_{inner}$ obtained from the PECAN analysis is the same as that found for hCox17$_{2S-S}$, whereas residues 35–46 in hCox17$_{outer}$ show a lower propensity to have a helical conformation (Fig. 3). The latter region comprises the last two turns of the N-terminal helix of the CHCH domain, the first turn of the C-terminal helix of the CHCH domain, and the 3_{10} helix between the two α-helical segments (Fig. 3).

The structure of hCox17$_{inner}$ is characterized by the CHCH domain with a root mean square deviation from the mean structure (residues 25–59) of 0.45 $\pm$ 0.19 Å for the backbone and 0.92 $\pm$ 0.17 Å for all heavy atoms. Although the outer disulfide bond is missing in hCox17$_{inner}$, the two α-helices get close to each other in an antiparallel conformation to form the same α-hairpin arrangement observed for the wild-type protein (Fig. 4*A*). 20 interhelical NOEs are observed between the side chains

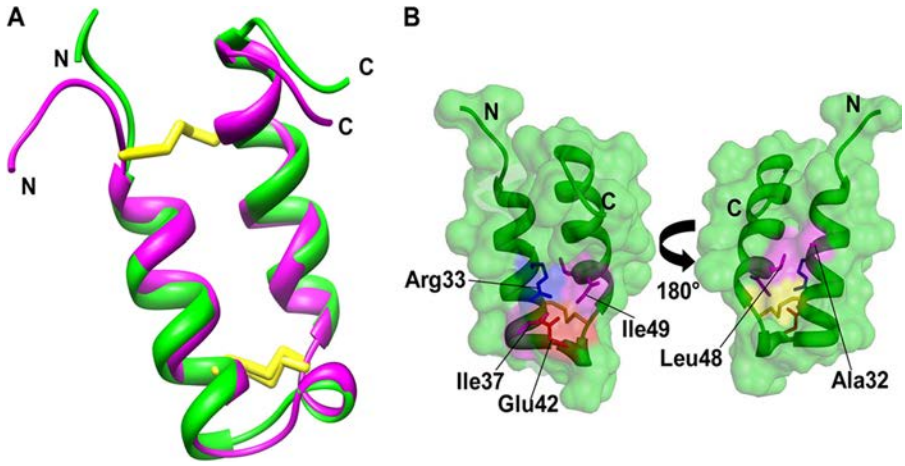

FIGURE 4. *A*, backbone superimposition of apo-hCox17$_{inner}$ (*green*) and apo-hCox17$_{2S\text{-}S}$ (*magenta*). The amino acids at the N termini of both proteins have been removed because they are completely unstructured. The cysteine residues are indicated in *yellow*. *B*, *ribbon diagram* of the lowest energy conformer of apo-hCox17$_{inner}$ with transparent surface representation in *green*. The hydrophobic residues involved in the stabilization of the α-hairpin fold are shown in *magenta*; Glu-42 and Arg-33 are shown in *red* and *blue*, respectively. The inner disulfide bond is shown in *yellow*.

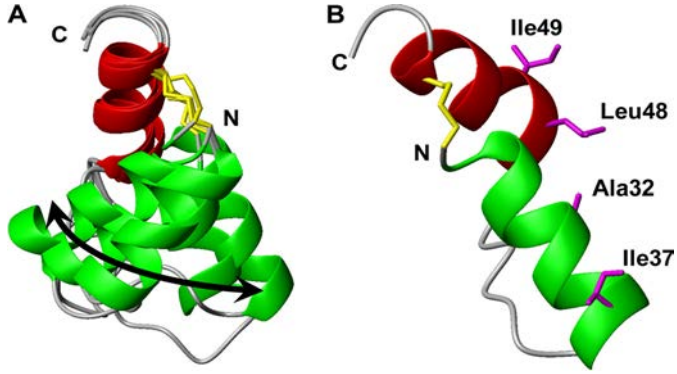

FIGURE 5. *A*, *ribbon representation* of five conformers of apo-hCox17$_{outer}$ obtained after CYANA structure calculations. Upon backbone superimposition of the second α-helix (in *red*), different relative orientations of the first α-helix (in *green*) are obtained. The outer disulfide bond is shown in *yellow*. *B*, hydrophobic residues involved in the stabilization of a single α-hairpin conformation in hCox17$_{inner}$ shown in *magenta* in a hCox17$_{outer}$ conformer.

of Ala-32, Arg-33, and Ile-37 (N-terminal helix) and the side chains of Leu-48, Ile-49 (C-terminal helix), and Glu-42 (3_{10} helix). The presence of the inner disulfide therefore determines the formation of a compact interhelical hydrophobic network and of a possible electrostatic interaction between the carboxylate group of Glu-42 and the guanidine group of Arg33 (Fig. 4*B*). These interhelical interactions envelop the inner disulfide bond, thus forcing the two helices close to each other in a unique conformational state.

The hCox17$_{outer}$ also has a CHCH fold. No interhelical NOEs are detected at variance with what is observed in the hCox17$_{inner}$, presumably as a result of different multiple conformations both in slow and fast exchange. The structure, calculated imposing the disulfide bond between the two helices and intrahelical NOEs, has a backbone root mean square deviation (residues 25–59) much higher than that of hCox17$_{inner}$ (3.07 $\pm$ 0.58 Å) (Fig. 5*A*). Another meaningful difference with respect to hCox17$_{inner}$ is the absence of the 3_{10} helix between the two α-helices as also shown by CSI (Fig. 5*A*). In hCox17$_{outer}$ the outer disulfide does not therefore determine a close packing of the interhelical residues as occurs in hCox17$_{inner}$. No hydrophobic interhelical contacts near the outer disulfide are indeed present. This is in agreement with the double conformations detected in the ^{1}H-^{15}N HSQC map of hCox17$_{outer}$ for several residues close to the disulfide bond, indicating the occurrence of a disulfide bond isomerization process. The hydrophobic contacts which are present in the vicinity of the inner disulfide in hCox17$_{inner}$ are also not formed in hCox17$_{outer}$ (Fig. 5*B*), in such a way so as not to be able to stabilize a single conformational state of the two helices but giving the protein the possibility of assuming different conformations in solution. The low number of NOE cross-peaks in the hCox17$_{outer}$ NOESY spectra with respect to those found in the hCox17$_{inner}$ NOESY spectra (see "Experimental Procedures") is consistent with this picture, *i.e.* that of a protein that has reasonably well defined secondary structural elements, but with a tertiary structure that fluctuates among widely different conformational arrangements.

To examine the effect of each disulfide bond on the copper binding properties of hCox17 protein, the metallated forms of both hCox17 mutants were studied by NMR and their copper(I) affinity compared with that of the wild-type protein. Chemical shift perturbation analysis of Cu(I)-hCox17$_{inner}$ *versus* apo-hCox17$_{inner}$ showed that metal binding determines large chemical shift changes as well as the generation of multiple conformations involving several residues surrounding the metal binding region, *i.e.* in the first turn of the N-terminal helix and in the C-terminal part of the second helix (Fig. 6, *A* and *B*). This behavior is drastically different from what is observed in the wild-type protein, in which, upon copper(I) binding, few residues close to the CC metal binding motif were affected, and no multiple conformations were induced by copper(I) binding (Fig. 6*C*) (10). On the contrary, the backbone chemical shifts of the outer mutant are affected by copper(I) binding similarly to what happens for the wild-type protein (Fig. 6*B*). Therefore, the local interactions near the metal binding site of hCox17 are influenced only by the lack of the outer disulfide bond, indicating its role in fine-tuning metal binding site structural environment. However, copper(I) binding affinities, measured by competitive titration against BCA, of hCox17$_{inner}$ and hCox17$_{outer}$ are similar to that of the wild-type protein (less than 1 order of magnitude of difference; supplemental Fig. S1), indicating that

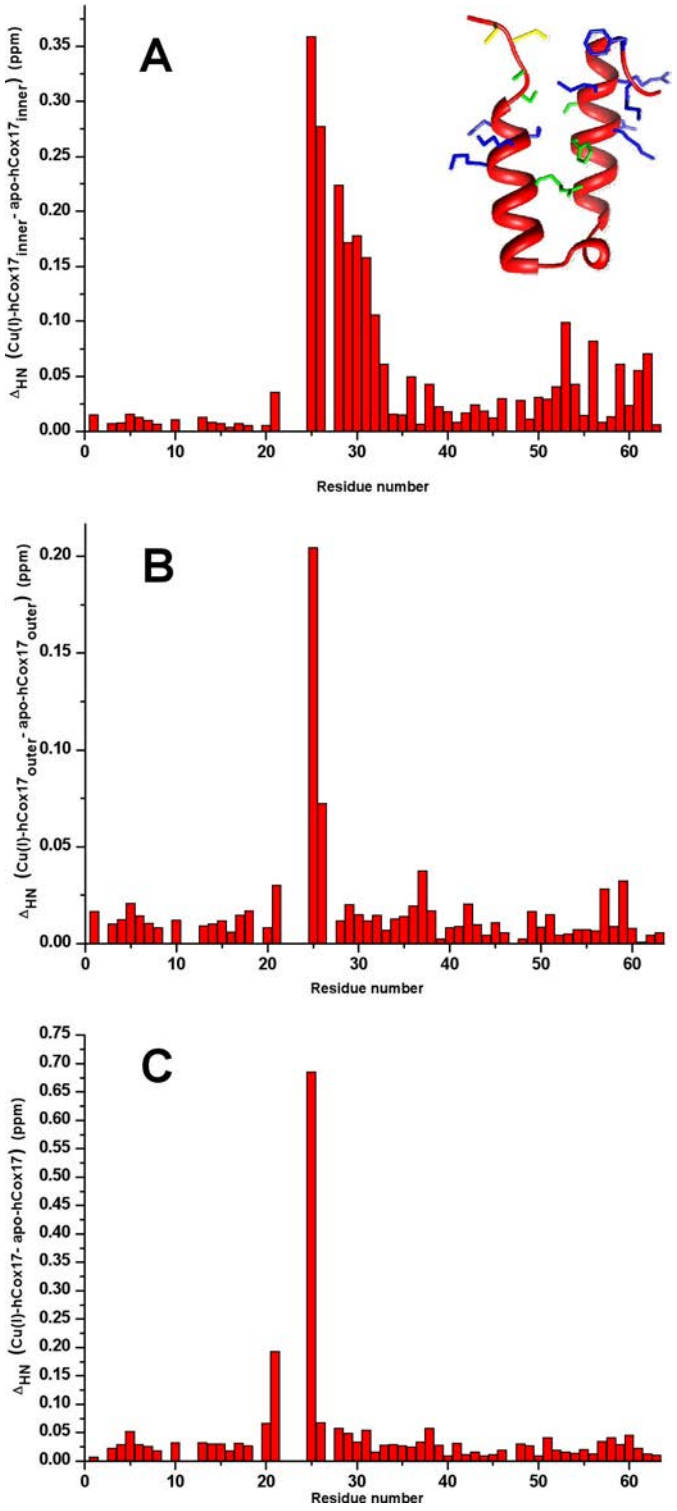

FIGURE 6. **Weighted-average backbone chemical shift differences ($((\Delta H)^2 + (\Delta N/5)^2)/2)^{1/2}$, where ΔH and ΔN are chemical shift differences for ^1H and ^{15}N, respectively) between Cu(I)-hCox17$_{inner}$ and apo-hCox17$_{inner}$ (*A*), Cu(I)-hCox17$_{outer}$ and apo-hCox17$_{outer}$ (*B*), and wild-type Cu(I)-hCox17$_{2S\text{-}S}$ and apo-hCox17$_{2S\text{-}S}$ (*C*).** In the inset of *A* the residues showing chemical shift variations above a threshold of 0.05 ppm and multiple conformations upon copper(I) binding are mapped in *blue* on the apo-hCox17$_{inner}$ structure. The residues showing just chemical shift variations above a threshold of 0.05 ppm are in *green*. The cysteine residues involved in copper(I) coordination are in *yellow*.

the removal of the inner or outer disulfide bond does not drastically affect the copper binding affinity of hCox17. This result is in agreement with normal levels of cytochrome *c* activity observed for yeast Cox17 mutants with Cys → Ser substitutions for the inner or outer cysteines (C47S and C57S, respectively) (13).

DISCUSSION

The lack of a disulfide bond in both the hCox17$_{inner}$ and hCox17$_{outer}$ mutants does not affect the CHCH structural topology present in the wild-type protein. However, different structural-dynamic properties are observed depending on whether the inner or the outer disulfide bond is formed. In hCox17$_{inner}$, the inner disulfide bond determines a network of specific contacts between the two helices and between them and the 3_{10}-loop region, all of these interactions surrounding the inner disulfide bond (Fig. 4*B*). All of the residues involved in these interactions are highly conserved and create in hCox17$_{inner}$ a hydrophobic patch that orients the two helices in a single conformational state, which is the same found when both disulfide bonds are present in the wild-type protein. By contrast, when only the outer disulfide bond is present, the two α-helices of the CHCH domain experience multiple reciprocal orientations, the helix 3_{10} is not formed (Fig. 5*A*), and conformational exchange processes are observed in helix α1 and in the following loop residues. The two α-helices in hCox17$_{outer}$ do not show any of the above-mentioned hydrophobic contacts observed in hCox17$_{inner}$ (Fig. 5*B*), and no further interhelical hydrophobic patches are present in the proximity of the outer disulfide bond, thus preventing the stabilization of a unique orientation of the two α-helices.

These structural-dynamic data on hCox17 Cys mutants therefore indicate that the inner disulfide bond is necessary and sufficient to determine the formation of a CHCH domain with essentially the same structural-dynamic properties of hCox17$_{2S\text{-}S}$. On the contrary, the same does not hold when only the outer disulfide bond is present. Consistent with the key structural role of the inner disulfide bond, hCox17$_{inner}$ unfolds upon the addition of 10 equivalents of DTT, whereas for hCox17$_{outer}$ 2 equivalents are sufficient to induce complete protein unfolding. All of these results contribute to the elucidation of the Mia40-induced oxidative folding mechanism of CX_9C Mia40 substrates (9, 16). Indeed, from these studies it has been found that the outer disulfide bond in the Mia40 substrates is formed only after generation by Mia40 of the inner disulfide bond, which, as we found in this work, is fundamental to generate the folding properties typical of the mature state of the protein.

The copper(I) binding-induced chemical shift changes on both mutants (Fig. 6) indicate that the outer disulfide bond, which is next to the Cys–Cys motif, is important for defining the local environment near the copper binding site. The copper(I) binding affinity of both mutants is, however, similar to that obtained for the wild-type protein. The hydrophobic contacts between Leu-20, Pro-22, Ala-25, Met-56, Leu-59, and Phe-61 have been proposed to play a role in wild-type Cu(I)-hCox17 in orienting Cu(I)-coordinating ligands through the formation of hydrophobic interactions (10). In wild-type apo-

hCox17 this hydrophobic patch is drastically reduced, Ala-25 being the only residue at the N terminus still interacting with the hydrophobic patch at the C terminus constituted by Met-56, Leu-59, and Phe-61 (10). In apo-hCox17$_{inner}$, the hydrophobic contacts between Met-56, Leu-59, Phe-61, and Ala-25 are conserved (10 NOE contacts between the hydrophobic side chains are present; in 70% of the 20 calculated conformers Ala-25 has hydrophobic contacts with Met-56, Leu-59, and Phe-61). In apo-hCox17$_{outer}$, the hydrophobic contacts between Met-56, Leu-59, and Phe-61 are present (7 NOE contacts between the hydrophobic side chains), but Ala-25 does not show NOEs with Met-56, Leu-59, or Phe-61, most likely as a consequence of the isomerization process of the outer disulfide bond which drastically reduces NOE detectability. In conclusion, the conservation of these hydrophobic contacts near the metal binding site can be a relevant factor contributing to the comparable metal binding affinities obtained for the mutants and the wild-type protein.

A mutational analysis of yeast Cox17 showed that cells harboring mutant Cox17 with conservative Cys → Ser substitutions for the inner cysteines are respiratory-competent and exhibit normal levels of cytochrome *c* oxidase activity (13). Our structure-based findings can interpret these functional data. Indeed, they show that the outer disulfide bond, which in yeast Cox17 is essential for its IMS import (15), determines a copper binding site structural arrangement and metal affinity similar to that which occurs in the wild-type protein, thus still allowing Cox17$_{outer}$ to work properly as a copper chaperone in the assembly process of the cytochrome *c* oxidase copper sites. Furthermore, because we have found that only one disulfide is sufficient to form both α-helices in a structural arrangement identical or similar to that of the wild-type protein, the conservative Cys → Ser substitutions for the inner cysteines do not drastically affect the folding properties in yeast Cox17, and consequently no cellular defects are observed even if the inner disulfide bond is not formed. On the contrary, when the nonconservative Cys → Arg substitution on the inner Cys-47 is introduced, the charge and the bulkiness of the Arg substitution can have a large effect on the protein folding properties, interfering with its function, and according to that, the Arg mutation determines completely respiration-deficient cells (20). Finally, yeast Cox17 is functional when the outer Cys-57 is substituted with a serine, but not functional when substituted with a tyrosine (13, 20). Our structural data can interpret the above findings. Indeed, the hydrophobic residues responsible for the single conformational state of the α-hairpin in hCox17$_{inner}$ (the same present in the wild-type protein) are conserved in yeast Cox17, and the conservative Ser mutation does not drastically perturb the copper binding site region. The metal affinity of hCox17$_{inner}$ is slightly lower than that of the wild-type protein, but not sufficient to determine a nonfunctional Cox17. On the contrary, the nonconservative Tyr mutation can drastically affect the conformational properties of the copper binding site region in such a way as to produce a nonfunctional yeast Cox17.

From this study, we conclude that the inner disulfide of hCox17 is the essential one for producing a single conformational state of the protein, playing a key structural role in the CHCH fold, whereas the outer disulfide bond defines the copper binding site structural environment of hCox17.

REFERENCES

1. Riemer, J., Bulleid, N., and Herrmann, J. M. (2009) *Science* **324,** 1284–1287
2. Depuydt, M., Messens, J., and Collet, J. F. (2011) *Antioxid. Redox. Signal.* **15,** 49–66
3. Hell, K. (2008) *Biochim. Biophys. Acta* **1783,** 601–609
4. Sideris, D. P., and Tokatlidis, K. (2010) *Antioxid. Redox. Signal.* **13,** 1189–1204
5. Herrmann, J. M., and Köhl, R. (2007) *J. Cell Biol.* **176,** 559–563
6. Banci, L., Bertini, I., Cefaro, C., Ciofi-Baffoni, S., Gallo, A., Martinelli, M., Sideris, D. P., Katrakili, N., and Tokatlidis, K. (2009) *Nat. Struct. Mol. Biol.* **16,** 198–206
7. Terziyska, N., Grumbt, B., Kozany, C., and Hell, K. (2009) *J. Biol. Chem.* **284,** 1353–1363
8. Mesecke, N., Terziyska, N., Kozany, C., Baumann, F., Neupert, W., Hell, K., and Herrmann, J. M. (2005) *Cell* **121,** 1059–1069
9. Banci, L., Bertini, I., Cefaro, C., Cenacchi, L., Ciofi-Baffoni, S., Felli, I. C., Gallo, A., Gonnelli, L., Luchinat, E., Sideris, D., and Tokatlidis, K. (2010) *Proc. Natl. Acad. Sci. U.S.A.* **107,** 20190–20195
10. Banci, L., Bertini, I., Ciofi-Baffoni, S., Janicka, A., Martinelli, M., Kozlowski, H., and Palumaa, P. (2008) *J. Biol. Chem.* **283,** 7912–7920
11. Palumaa, P., Kangur, L., Voronova, A., and Sillard, R. (2004) *Biochem. J.* **382,** 307–314
12. Arnesano, F., Balatri, E., Banci, L., Bertini, I., and Winge, D. R. (2005) *Structure* **13,** 713–722
13. Heaton, D., Nittis, T., Srinivasan, C., and Winge, D. R. (2000) *J. Biol. Chem.* **275,** 37582–37587
14. Heaton, D. N., George, G. N., Garrison, G., and Winge, D. R. (2001) *Biochemistry* **40,** 743–751
15. Sideris, D. P., Petrakis, N., Katrakili, N., Mikropoulou, D., Gallo, A., Ciofi-Baffoni, S., Banci, L., Bertini, I., and Tokatlidis, K. (2009) *J. Cell Biol.* **187,** 1007–1022
16. Bien, M., Longen, S., Wagener, N., Chwalla, I., Herrmann, J. M., and Riemer, J. (2010) *Mol. Cell* **37,** 516–528
17. Voronova, A., Meyer-Klaucke, W., Meyer, T., Rompel, A., Krebs, B., Kazantseva, J., Sillard, R., and Palumaa, P. (2007) *Biochem. J.* **408,** 139–148
18. Banci, L., Bertini, I., Ciofi-Baffoni, S., Kozyreva, T., Zovo, K., and Palumaa, P. (2010) *Nature* **465,** 645–648
19. Maxfield, A. B., Heaton, D. N., and Winge, D. R. (2004) *J. Biol. Chem.* **279,** 5072–5080
20. Punter, F. A., and Glerum, D. M. (2003) *J. Biol. Chem.* **278,** 30875–30880
21. Banci, L., Bertini, I., Ciofi-Baffoni, S., Leontari, I., Martinelli, M., Palumaa, P., Sillard, R., and Wang, S. (2007) *Proc. Natl. Acad. Sci. U.S.A.* **104,** 15–20
22. Banci, L., Bertini, I., Ciofi-Baffoni, S., Hadjiloi, T., Martinelli, M., and Palumaa, P. (2008) *Proc. Natl. Acad. Sci. U.S.A.* **105,** 6803–6808
23. Horng, Y. C., Cobine, P. A., Maxfield, A. B., Carr, H. S., and Winge, D. R. (2004) *J. Biol. Chem.* **279,** 35334–35340
24. Punter, F. A., Adams, D. L., and Glerum, D. M. (2000) *Hum. Genet.* **107,** 69–74
25. Keller, R. (2004) *The Computer Aided Resonance Assignment Tutorial*, CANTINA Verlag, Goldau
26. Herrmann, T., Güntert, P., and Wüthrich, K. (2002) *J. Mol. Biol.* **319,** 209–227
27. Herrmann, T., Güntert, P., and Wüthrich, K. (2002) *J. Biomol. NMR* **24,** 171–189
28. Shen, Y., Delaglio, F., Cornilescu, G., and Bax, A. (2009) *J. Biomol. NMR* **44,** 213–223
29. Sharma, D., and Rajarathnam, K. (2000) *J. Biomol. NMR* **18,** 165–171
30. Case, D. A., Darden, T. A., Cheatham, T. E., Simmerling, C. L., Wang, J., Duke, R. E., Luo, R., Merz, K. M., Wang, B., Pearlman, D. A., Crowley, M., Brozell, S., Tsui, V., Gohlke, H., Mongan, J., Hornak, V., Cui, G., Beroza, P., Schafmeister, C. E., Caldwell, J. W., Ross, W. S., and Kollman, P. A. (2008) AMBER 10 (8.0), University of California, San Francisco, CA
31. Bhattacharya, A., Tejero, R., and Montelione, G. T. (2007) *Proteins* **66,**

778–795
32. Vriend, G. (1990) *J. Mol. Graphics* **8,** 52–56
33. Zhou, L., Singleton, C., and Le Brun, N. E. (2008) *Biochem. J.* **413,** 459–465
34. Siluvai, G. S., Nakano, M., Mayfield, M., and Blackburn, N. J. (2011) *J. Biol. Inorg. Chem.* **16,** 285–297
35. Xiao, Z., Brose, J., Schimo, S., Ackland, S. M., La Fontaine, S., and Wedd, A. G. (2011) *J. Biol. Chem.* **286,** 11047–11055
36. Otting, G., Liepinsh, E., and Wüthrich, K. (1993) *Biochemistry* **32,** 3571–3582
37. Wishart, D. S., and Sykes, B. D. (1994) *J. Biomol. NMR* **4,** 171–180
38. Eghbalnia, H. R., Wang, L., Bahrami, A., Assadi, A., and Markley, J. L. (2005) *J. Biomol. NMR* **32,** 71–81
39. Pettersen, E. F., Goddard, T. D., Huang, C. C., Couch, G. S., Greenblatt, D. M., Meng, E. C., and Ferrin, T. E. (2004) *J. Comp. Chem.* **25,** 1605–1612

Table S1. Statistical analysis of the energy minimized family of conformers of $hCox17_{inner}$.

	AMBER 10.0[a]
RMS deviations per meaningful distance constraint (Å)[b]:	(20 structures)
Intraresidue (158)	0.0065 ± 0.0063
Sequential (149)	0.0208 ± 0.0062
Medium range (206)[c]	0.0198 ± 0.0031
Long range (24)	0.0106 ± 0.0122
Total (537)	0.0178 ± 0.0015
RMS violations per meaningful dihedral angle constraints (deg)[b]:	
Phi (46)	1.20 ± 1.01
Psi (46)	6.17 ± 4.19
Average no. of NOE violations larger than 0.3 Å	0.05 ± 0.22
Average NOE deviation ($Å^2$)[d]	0.21 ± 0.03
Average angle deviation (rad^2)[d]	0.16 ± 0.10
RMSD to the mean structure (Å) (BB)[e] (HA)[e]	0.51 ± 0.21 1.16 ± 0.15
Structural analysis	
% of residues in most favorable regions[f, g]	87.2%
% of residues in allowed regions[f, g]	12.7%
% of residues in generously allowed regions[f, g]	0.2%
% of residues in disallowed regions[f, g]	0.0%
G-factor[f, g]	0.12 ± 0.04
Structure Z-scores[g, h]	
1st generation packing quality	1.6
2nd generation packing quality	4.8
Ramachandran plot appearance	-1.6
$\chi1/\chi2$ rotamer normality	-4.0
Backbone conformation	-0.2
RMS Z-Score[g, h]	
Bond lengths	1.2
Bond angles	0.7
Omega angle restraints	1.3
Side chain planarity	1.2
Improper dihedral distribution	1.2
Inside/Outside distribution	1.1

[a]AMBER indicates the energy minimized family of 20 structures.
[b]The number of meaningful constraints for each class is reported in parenthesis.
[c]Medium range distance constraints are those between residues (i,i+2), (i,i+3), (i,i+4) and (i,i+5).
[d]NOE and torsion angle constraints were applied with force constants of 20 kcal mol^{-1} $Å^{-2}$, 20 kcal mol^{-1} rad^{-2}, respectively.
[e]The RMSD to the mean structure is reported considering the segment 25-62.
[f]As it results from the Ramachandran plot analysis. For the PROCHECK statistics, an overall G-factor larger than -0.5 are expected for a good quality structure.
[g]The statistic analysis is reported considering the segment 25-62.
[h]Values based on WHAT-IF output. A Z-score is defined as the deviation from the average value for this indicator observed in a database of high-resolution crystal structures, expressed in units of the standard deviation of this database-derived average. Typically, Z-scores below a value of -3 are considered poor, those below -4 are considered bad.

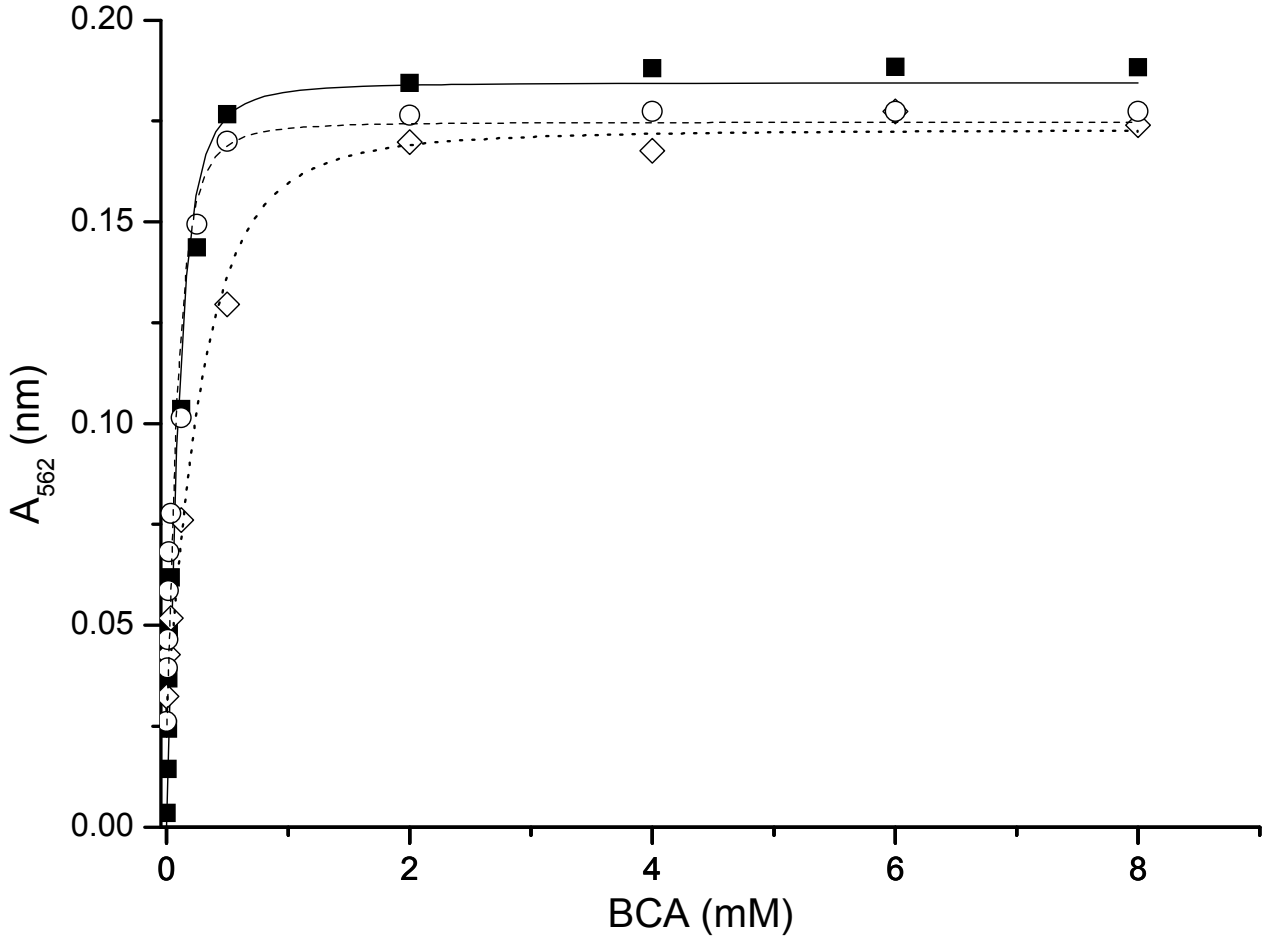

Fig. S1. Fitting of the data for the titrations of wild-type Cu(I)-hCox17 (◊), Cu(I)-hCox17$_{inner}$ (○) and Cu(I)-hCox17$_{outer}$ (■) with BCA concentrations ranging from 0 to 8 mM with Origin 8.1 to calculate the association constants (8.8×10^{16} M^{-1}, 1.2×10^{16} M^{-1} and 1.3×10^{16} M^{-1}, respectively). The data were simulated using a β_2 association constant of Cu(I)-BCA equal to 2.0×10^{17} M^{-1}.

Functional Role of Two Interhelical Disulfide Bonds in Human Cox17 Protein from a Structural Perspective

Lucia Banci, Ivano Bertini, Chiara Cefaro, Simone Ciofi-Baffoni and Angelo Gallo

J. Biol. Chem. 2011, 286:34382-34390.
doi: 10.1074/jbc.M111.246223 originally published online August 4, 2011
